8758 *Biochemistry* **2009,** *48,* 8758–8763
DOI: 10.1021/bi9007808

BIOCHEMISTRY
including biophysical chemistry & molecular biology
Article

Ion-Blocking Sites of the Kir2.1 Channel Revealed by Multiscale Modeling[†]

Kaihsu Tai, Phillip J. Stansfeld, and Mark S. P. Sansom*

Department of Biochemistry, University of Oxford, South Parks Road, Oxford OX1 3QU, United Kingdom

Received May 6, 2009; Revised Manuscript Received July 29, 2009

ABSTRACT: The Kir2.1 potassium channel owes its inward-rectifying behavior to blocking by multivalent ions, e.g., magnesium and spermine, which access the channel from the cytoplasm and are thought to bind within the pore. To investigate the pathway followed by these ions from the cytoplasm through the pore, we have used multiscale modeling (via continuum electrostatics calculations, docking, and molecular dynamics simulations) to identify possible binding sites en route. On its way to eventually binding in the cavity, magnesium interacts extensively with Glu299, which lines the pore in the center of the intracellular domain. Interaction sites for spermine are formed by Asp255, Glu299, and Glu224. Entropic factors seem to favor interactions of spermine within the center of the cytoplasmic domain.

Kir2.1 (also known as IRK1, gene *KCNJ1*) is a member of the Kir2.x inward-rectifying potassium channel family and is mainly responsible with other Kir2.x channels for the inward rectifier current I_{K1} in the human heart ventricle (*1*, *2*). This current stabilizes the resting membrane potential and shapes the final repolarization of the ventricular action potential. Abnormality of this current has been implicated in long and short QT syndromes, alterations of cardiac excitability, and ventricular and atrial fibrillation (*3*). Kir2.1 itself has been associated with Andersen's syndrome, hypertension, and cardiomyopathies. Kir2.1 exhibits voltage-dependent rectification which is thought to be due to pore block by multivalent ions from the cytosol, e.g., magnesium (Mg^{2+}) or polyamines such as spermine and spermidine.

Like many other K^+ channels, Kir2.1 is a homotetramer (Figure 1). Like other inward-rectifying channels, it has two domains in each monomer: transmembrane and cytoplasmic. In the transmembrane domain, there is a filter region closest to the extracellular mouth. Kir2.1 shares with other K^+ channels the signature sequence in the filter region, "T(I/V)GYG". Along the pore and next to the filter is a large cavity marked by Asp172, which is likely to be filled with several water molecules and possibly some ions. Next to the cavity toward the cytoplasmic domain, there is the main gate formed by Met180. The blocking ions (Mg^{2+} and polyamines), subjects of this investigation, are thought to enter the cytoplasmic domain, pass the gates, and bind within the cavity (*4*−*6*).

Crystallographic structures for the cytoplasmic domain of Kir2.1 have appeared (*7*, *8*), but not for the transmembrane domain. A homology model for both domains of the related Kir3.1 (*9*) has been published. Crystallographic structures for a chimera of mouse Kir3.1 and KirBac1.3 (PDB[1] entry 2QKS, 2.2 Å resolution) have recently appeared (*10*). Within the same crystal, two conformations of the cytoplasmic domain were observed, differing in the conformation of a possible second gate at Met307 (not to be confused with the main M2 helix bundle crossing gate at Met180). These have been identified as being in a "dilated" conformation and a "closed" conformation with respect to the possible second gate (*10*). We used these as templates to prepare two models of human Kir2.1: one in a Met307-dilated state and another in a Met307-closed state. So far, a structure with the main M2 bundle crossing (i.e., Met180) gate open has not been modeled as a suitable template is not available.

MATERIALS AND METHODS

Homology Modeling. The crystallographic structure of the Nishida Kir3.1/KirBac1.3 chimera (*10*) was used as a template for modeling human Kir2.1. The sequence alignment was performed using Jalview 2.2 (*11*) and MUSCLE (*12*) and is shown in Figure S1 of the Supporting Information (48% sequence identity). Modeller 9v2 (*13*) was used to make the initial model for Kir2.1, with 4-fold symmetry restraints and restraints on the salt bridge behind the filter between the side chains of Glu138 and Arg148. Procheck (*14*) was used to check the model; VMD (*15*) was used to inspect it visually. VOIDOO and FLOOD (*16*) identified cavities in the Kir2.1 models and filled these with water molecules.

Electrostatic Calculations. At a coarse-grained level, one may investigate channel−ion interactions via electrostatics calculations involving solution of the Poisson−Boltzmann (PB) equation (*17*). Thus, we used Adaptive Poisson−Boltzmann Solver (APBS) (*18*) to calculate the electrostatic energy profile (*19*) of a Mg^{2+}, spermine, or spermidine ion as a function of position along the central pore axis of each of the two models. The pore axis and radius profile for each model were defined by HOLE (*20*) with the XPLOR radius parameters (suitable for united atoms) to identify sample points along the pore. The sample points in the pore were placed at 1 Å z intervals.

For a calculation at a sample point, a magnesium ion (Mg^{2+}) with a radius of 1.455 Å (*21*) was placed along the pore axis, which extends from beneath the cytoplasmic domain (z = 20 Å) to beyond the extracellular mouth of the pore (z = 120 Å), thus

[†]This research is funded by the Wellcome Trust.
*To whom correspondence should be addressed. Phone: +44 1865 613306. Fax: +44 1865 613238. E-mail: mark.sansom@bioch.ox.ac.uk.
[1]Abbreviations: APBS, Adaptive Poisson−Boltzmann Solver; KDB, Potassium Channel Database; Kir, inward-rectifying potassium channel; MD, molecular dynamics; PB, Poisson−Boltzmann; PDB, Protein Data Bank.

 Published on Web 08/04/2009 © 2009 American Chemical Society

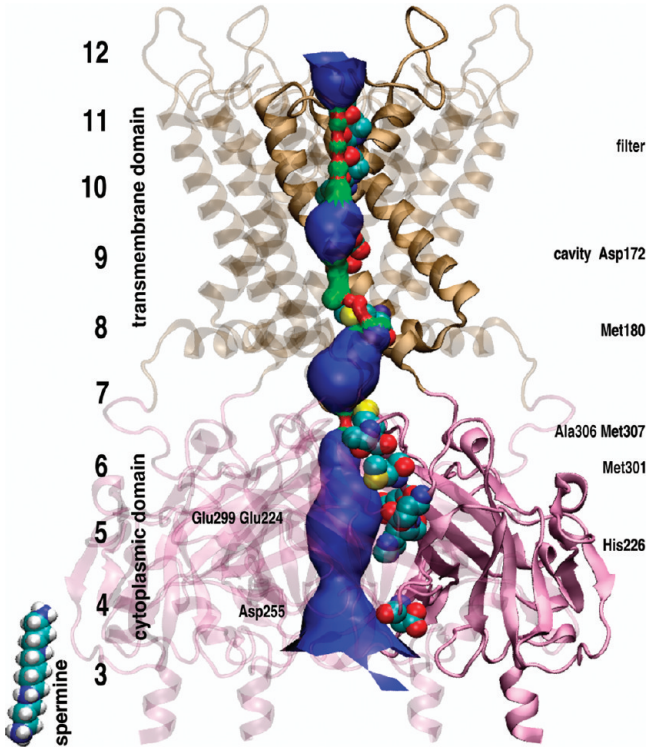

FIGURE 1: Kir2.1 channel model. Key side chains are shown in space-filling format. The pore-lining surface is shown. A spermine molecule is shown for scale.

covering a length of 100 Å. The likely spermine and spermidine binding sites were explored with a similar method. Spermidine has the structure H_3N^+-$(CH_2)_4$-$^+NH_2$-$(CH_2)_3$-$^+NH_3$, and spermine H_3N^+-$(CH_2)_3$-$^+NH_2$-$(CH_2)_4$-$^+NH_2$-$(CH_2)_3$-$^+NH_3$. In our calculations of PB energy profiles, spermidine was modeled as three amino groups (each with a $+1e$ point charge, 2.13 Å radius) in a line, spaced at 6.30 Å ("butane" end) and 5.00 Å ("propane" end); the reference point was the middle amino group. Spermine was modeled as four amino groups, spaced at 5.00, 6.30, and then 5.00 Å in a line; the reference point was the center of the middle butane stretch.

PB calculations were performed on these models at all sample points, using APBS in combination with PDB2PQR (*22*) and the AMBER99 force field (*23*). A grid of 97 × 97 × 193 points was placed on a cuboid with dimensions of 120 Å × 120 Å × 180 Å. The temperature in the APBS calculations was set to 300 K, and an ambient electrolyte concentration of 0.15 M NaCl was selected, to be comparable to physiological conditions. The electrostatic free energy of solvation was evaluated at each sample point for either model.

Molecular Dynamics Simulations without Spermine. To explore the effects of protein dynamics on the electrostatic energy profile, we performed three molecular dynamics (MD) simulations, each starting from a slightly different starting conformation of the Met307-closed Kir2.1 model with a duration of 20 ns. Snapshots from these simulations thus served as additional models from which to generate electrostatic energy profiles.

The homology models were subject to energy minimization using the steepest-descent and conjugate-gradient algorithms, implemented in Gromacs (*24*). The MD simulations were conducted with only the homology model in the closed conformation. This model has 323 residues in each of the four chains, with a total charge of $-24e$ ($-6e$ per chain). In the filter, a potassium ion was placed at each of sites 2 and 4; a water molecule is placed at each of sites 0, 1, and 3. A POPC bilayer was solvated in a box of water molecules large enough to contain the Kir2.1 model. This was energy minimized (steepest descent and then conjugate gradient) and then equilibrated using MD at 100 K for 100 ps, 200 K for 100 ps, and then 310 K for 1 ns, all with 2 fs time steps.

The closed-state model was then inserted into the bilayer using Gromacs tools. The result of the insertion was visually inspected using VMD to ensure the protein is placed at an appropriate place along the bilayer normal. This is considered to be achieved when the Arg and Lys residues are near the headgroups of the lipids, and the Tyr and Trp residues are at interfacial locations. To confirm, we performed coarse-grained MD simulations (*25*) to allow lipid self-assembly into bilayers around a coarse-grained version of our Kir2.1 model. The results from these corroborated our identification of bilayer location.

The system, with the Kir2.1 model inserted, had 141 potassium cations (including those in the pore) and 117 chloride anions. The resulting box had approximate dimensions of 124 Å × 136 Å × 158 Å, with 208752 atoms in total. It was an electrically neutral system with 88 mmol/dm^3 K^+ and 73 mmol/dm^3 Cl^-. This compares with the physiological intracellular composition on the order of 102 mmol/dm^3 for each of these species.

The system with Kir2.1 inserted was energy minimized (steepest descent and then conjugate gradient), holding the protein's position fixed, and then equilibrated using MD, still holding the protein fixed, using 1 fs time steps, at 100 K for 100 ps, 200 K for 100 ps, and 310 K for 100 ps. The thermostat (relaxation time of 0.1 ps) and semi-isotropic barostat (100 kPa, relaxation time of 1.0 ps, compressibility of 4.5 Pa^{-1}) were of the Berendsen type (*26*). The electrostatics treatment at this stage was Coulombic with a 14 Å cutoff.

The position restraints on the protein were then removed; the whole system was further equilibrated with restraints on the protein backbone atoms only (releasing restraints on the side chain protein atoms) with 1 fs time steps for 100 ps, and then with restraints on the α-carbon atoms only (releasing the restraints on other backbone atoms). The electrostatics treatment from this stage onward was particle-mesh Ewald (*27*).

Four production runs were conducted (see Table 1 of the Supporting Information, after ref *28*), each with a different number of potassium ions in the cavity region: with no ions, with one potassium ion, with three potassium ions, and with seven potassium ions. The starting configurations for each of these were obtained by swapping a water molecule in the cavity with a potassion ion in bulk water. In addition, a fifth simulation which started with the configuration (without ions in the cavity) not subjected to the backbone- and α-carbon-restrained equilibration described above was conducted.

All five production runs were at 310 K, without restraints, with 2 fs time steps, for 20 ns each. The resulting trajectories were deposited into KDB (*29*) and BioSimGrid (*30*); the accession codes are given in Table 2 of the Supporting Information.

Molecular Dynamics Simulations with Spermine. We conducted three MD simulations [using Gromacs v3 (*24*)] with spermine initially situated at the Glu299 site in Kir2.1 and observed the interactions in the binding pocket. The first simulation was in vacuo for 1 ns; in the latter two, the spermine−Kir2.1 system was embedded in a POPC bilayer and solvated in water.

The molecular mechanics parameters for spermine were supplied with PRODRG (*31*) and the resulting interactions

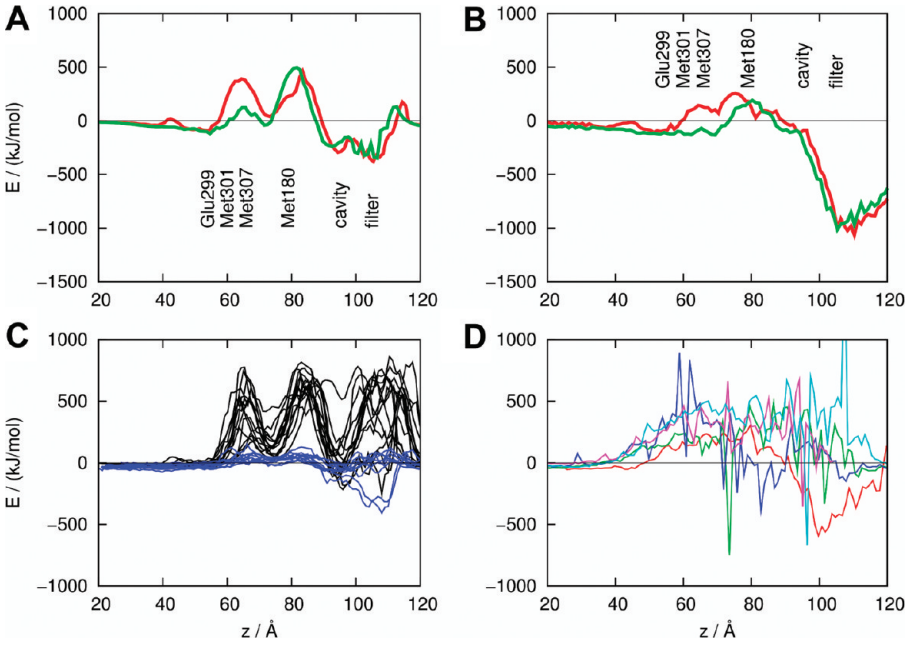

FIGURE 2: Profiles of Poisson−Boltzmann electrostatic energies for ions in the Kir2.1 pore. In panels A and B, each pair of curves is for a cytoplasmically closed (red) and an open (green) Kir2.1 homology model: (A) Mg^{2+} and (B) spermine. (C) Profiles from molecular dynamics snapshots: Mg^{2+} (black, 15 snapshots) and K^+ (blue, 10 snapshots). (D) Profiles for spermine from five molecular dynamics snapshots.

generated using LIGPLOT (*32*). To optimize the spermine binding site, Gromacs was used to perform energy minimization of the spermine−Kir2.1 complex, with spermine placed and restrained in the most favorable position as presented by PB calculations. Then 1 ns of MD in vacuo was conducted using the Gromacs 43b1 (vacuum) force field and the Gromacs 3.2.1 software.

To observe the exploration of binding poses by spermine, two more MD simulations with Kir2.1 embedded in a lipid bilayer and water-solvated were conducted for 20 ns with Gromacs 3.3. In one, the starting conformation was the same as the one described above with one potassium ion in the cavity; in addition, spermine was placed at the most favorable position as presented by PB calculations. In the other, spermine was placed in the cavity.

Mutation. For the preparation of the Glu224Gly, Glu299Ser, Arg228Gln, and Arg260Gln mutants, WHAT IF (*33*) was used to mutate the residues and remove possible steric collisions.

Docking. To complement this method of binding site exploration, AutoDock 4 (*34*) was used to perform 100 Lamarckian genetic algorithm local searches, each with 106 steps of energy evaluations. A set of global searches with otherwise the same parameters were also conducted.

RESULTS AND DISCUSSION

Figure 2A shows the PB energy barrier encountered by a Mg^{2+} ion traversing the pore. The difference in barrier height due to the dilation of the Met307 gate is 66 Å (z). A further constriction appears at 60 Å due to the M2 bundle crossing gate at Met301. Thus, a Mg^{2+} ion approaching from the cytoplasm can find an energetically favorable position for binding to Kir2.1 and blocking the K^+ current by interacting with Glu299 (z = 54 Å). The Met307 barrier (z = 66 Å) makes the Mg^{2+} less likely to reach the next energetically favorable position at 74 Å. The Mg^{2+} ion encounters the Met180 barrier at 80 Å before reaching the cavity. The residue of most interest here, Glu299, is well-conserved among inward-rectifying potassium channels. It corresponds to Asp297 of Kir1.1, Glu288 of Kir6.2, and a glutamic acid in the Kir3.1/KirBac1.3 chimera, all residues prone to similar interactions with Mg^{2+}. This is close to the G-loop (residues 301−311), thought to regulate rectification and gating from the cytoplasmic domain (*7*, *8*).

The dynamics of the channel seems to weaken binding from −100 to −30 kJ/mol at Glu299 (Figure 2C). In a dynamic situation, the four copies of the Glu299 residue are too far apart to position themselves as well to form a definite Mg^{2+} binding site as in the static homology model. (It must be borne in mind that these MD simulations were conducted in the absence of the Mg^{2+} ions in the binding site; it does not rule out the possibility of binding site residues reconstituting themselves in the presence of a Mg^{2+} ion along the lines of induced-fit models.)

Figure 2B shows the resulting PB energy profiles for spermine in the closed and open models of Kir2.1. Results for spermidine (not shown) are similar in the cytoplasmic domain. For both ligands in the closed model, the favorable energy occurs when the pioneering ammonium group reaches the Glu299 site; this is not much different from Mg^{2+} binding, with a similar magnitude of favorable energy, −100 kJ/mol. More interesting is the binding in the Met307 dilated model, where a deeper energy well of −150 kJ/mol appears to extend even to the Met307 gate. However, the barrier at the Met180 gate remains at 200−300 kJ/mol in the closed state and 100 kJ/mol in the dilated state, suggesting that the latter is more susceptible to polyamine overcoming the Met180 barrier to reach the cavity. In a dynamic situation (Figure 2D), binding sites in the static models that appear well-defined for spermine were all but abolished. However, we will show below that blocks of current by spermine do not necessarily call for a well-defined binding site.

The electrostatics calculations showed favorable binding energies with Mg^{2+} (−300 kJ/mol) in the cavity near Asp172 suggested previously (*4*−*6*), and spermine (−1 MJ/mol) in the filter. This indicates the most favorable location for binding if only electrostatic enthalpy is considered. However, we also

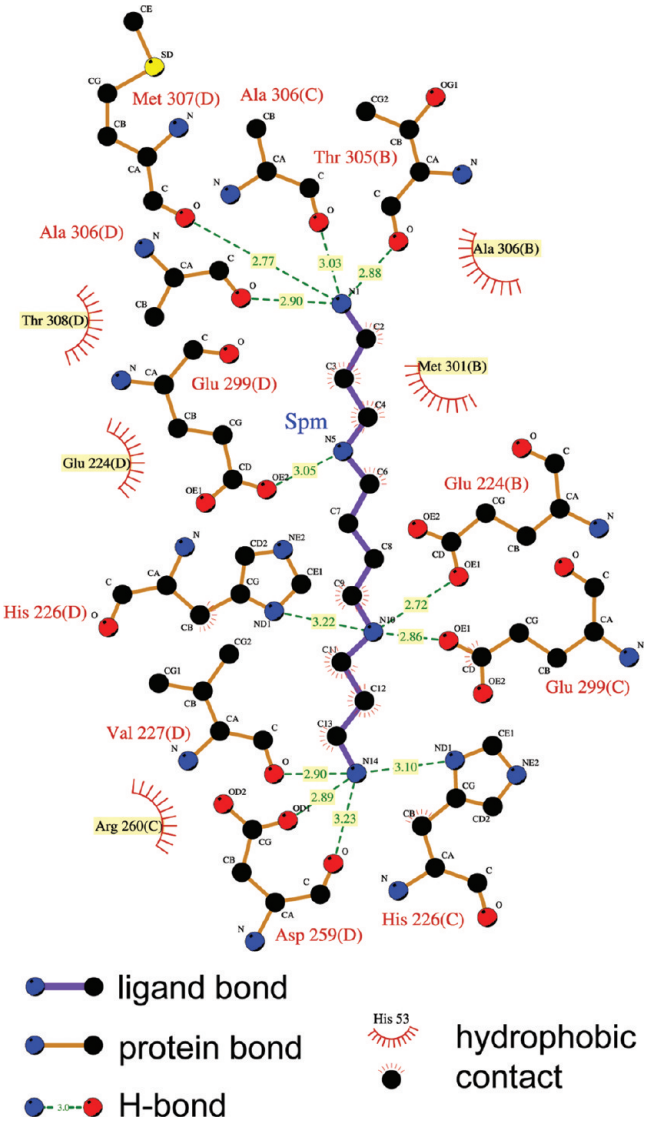

FIGURE 3: Cytoplasmic binding site for spermine: interactions between Kir2.1 and spermine (Spm) after 1 ns of in vacuo molecular dynamics. Produced with Ligplot (*32*).

explored the entropic implications to the binding process of spermine (and similar polyamines) with MD and docking studies. First, AutoDock identified 38 clusters of docking conformations near Glu299. Each of the clusters had a contact with Asp255, indicating the significance of Asp255 in interacting with a spermine molecule within the cytoplasmic section of the pore.

From the trajectory in vacuo (1 ns snapshot in Figure 3), we can see that the following residues are prominent for the retention of the spermine molecule in this binding pose. For the pioneering ammonium group, the backbone oxygen atom of Ala306 is prominent in hydrogen bonding, along with interactions by the backbone atoms of neighboring residues such as Thr305 and Met307. The side chain oxygen atom of Thr308 forms hydrogen bonds with the second ammonium group. Glu224 and Glu299, which form hydrogen bonds with the second and third ammonium groups from time to time, have also been mentioned in the literature recently (*35*) as having "significant long-range effects on the electrostatic profile throughout the channel". Finally, His226 forms a hydrogen bond with the third and fourth ammonium groups. The pore profile as determined by HOLE (data not shown) indicates that spermine thus bound sterically

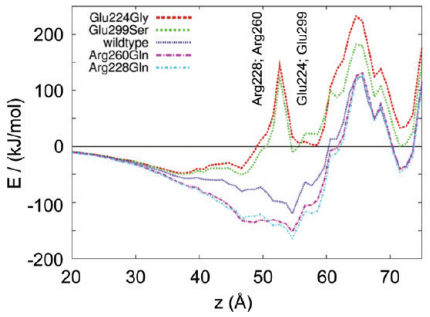

FIGURE 4: Profiles of Poisson−Boltzmann electrostatic energies for Mg^{2+} in the pores of the mutant Kir2.1 cytoplasmic domain. From top to bottom: Glu224Gly, Glu229Ser, wild type, Arg260Gln, and Arg228Gln.

blocks potassium ion permeation by completely abolishing the pore through the vestibule in the cytoplasmic domain.

This in vacuo map provides an initial approximation for identifying the key residues underlying block by spermine. First, the spermine molecule is attracted to the mouth of the pore, where Asp255 plays a major role. Then, the ammonium groups on the spermine make contact with the following residues each located yet deeper in the pore than the previous one: His226, Glu299, Glu224, and the backbone atoms near Ala306. Some of these residues, Glu299, Glu224, and Asp255 (along with Asp259, not seen here), had been implicated in mutation studies as influencing spermine-induced rectification (*36*). The two sets of glutamic acid residues contribute to the overall electrostatic profile in addition to specific hydrogen bonding interactions (*35*). The residues around Ala306 are within the regulatory G-loop mentioned above. Together, these residues form a favorable binding region between the cytoplasm and the cavity.

We note that this initial approximation does not preclude the possibility of two spermine molecules binding to Kir2.1, despite their anticipated mutual repulsion due to the high positive charge of $+4e$ on each molecule. One possibility is for a first spermine to progress along the pore to bind in the cavity, and a second following, bound in the cytoplasmic domain: this being the "long-pore plugging" hypothesis (*35*, *37*). Another possibility, which we have observed in an earlier modeling work on a different Kir2.1 model (based on a Kir3.1 structure, PDB entry 1N9P), places two spermine molecules perpendicular to the pore, each interacting with two copies of Glu224 and Glu299 in the tetramer (*38*).

Earlier mutation studies found that neutralizing the negatively charged Glu224 and Glu299 decreases the blockers' affinity (*39*−*42*). Further, in addition to His226 reported here, positively charged residues Arg228 and Arg260 decrease the affinity for cations (*35*, *43*). To probe these effects in silico, we conducted PB calculations for the following mutants: Glu224Gly, Glu299Ser, Arg228Gln, and Arg260Gln. The PB profiles for Mg^{2+} in the cytoplasmic pores of in silico mutants (Figure 4) confirm these observations. Removing negatively charged glutamate residues at Glu224 or Glu299 abolishes much of the cytoplasmic vestibule site for a cation, whereas replacing positively charged arginine residues such as Arg228 and Arg260 with glutamine enhances it.

In the trajectory with the Kir2.1 domain embedded in a lipid bilayer, the spermine explored various poses in the cytoplasmic domain during the 50 ns. Many, but not all, of the residues forming hydrogen bonds with spermine (Figure 5A) corresponded to those seen in the in vacuo simulation. Spermine never ventured into the transmembrane domain, let alone the specific, favorable cavity binding site near Asp172. Another 20 ns

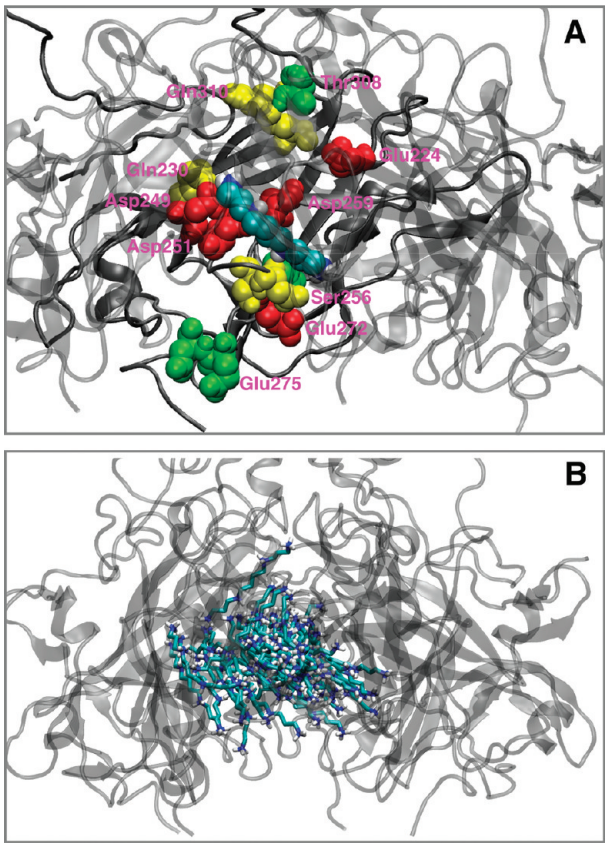

FIGURE 5: (A) Residues forming hydrogen bonds with spermine, as observed in the 5000 frames in the 50 ns trajectory. The five red residues formed 576 (Asp249) to 1338 (Glu224) hydrogen bonds. The yellow ones formed 106−510; the green formed fewer than 84. For the sake of clarity, the hydrogen bond counts are summed over all monomers but only a snapshot of one monomer is shown. (B) Fifty binding conformations, sampled every 1 ns, explored by spermine in the same 50 ns trajectory.

trajectory with spermine starting from the cavity immediately ejected that polyamine into the cytoplasmic domain. These bring us to the final conclusion of this study: Though the cavity location is the most enthalpically favorable position for spermine to bind, as postulated in the crystallographic structure for KirBac3.1 (*6*), this binding mode allows only one degree of freedom (i.e., rotational). In the cytoplasmic domain, there are many possible, nonspecific binding poses for spermine to adopt (sketched out in Figure 5B), some far from alignment along the pore axis and some even with spermine adopting incompletely extended conformations. These poses may be less favorable in enthalpy, but the multiplicity more than compensates in entropy.

In analyzing these interactions, we must remember that their will be a degree of sensitivity of the channel−spermine interactions to the initial side chain conformations assigned during the homology modeling process. However, one should also recall that in MD simulations, the side chains of these residues are able to reorient according to the dynamic fluctuations in their environment (including changes in the conformation of the spermine molecule), thus "relaxing" initial side chain conformer assignments from the homology modeling. That such relaxation occurs can be seen from analysis of side chain torsion angles for residues interacting with spermine over the course of a 50 ns MD simulation of the Kir2.1−spermine complex (see the Supporting Information).

In thinking of a design for effective blockage by spermine, it is tempting to opt for an enthalpically strong binding site for spermine by lining a cavity of the right size with strong negative charges. However, this could weaken the spermine molecule's effectiveness in repelling other cations, such as the current-carrying potassium ions. It is therefore more effective to have a wider region of diffused negative charges for spermine to move around. The two principal gains are (i) spermine retains much of its four cation-repelling positive charges and (ii) spermine pays a smaller penalty in entropy reduction upon its binding to Kir2.1. The balance between entropic and enthalpic effects, and their ultimate implications in rectification by selective blockage of current, are amenable to computational approaches and await a further study with Brownian dynamics and free energy calculations.

ACKNOWLEDGMENT

We thank Oliver Beckstein, Martin Fink, Philip Fowler, Peter Hunter, Younes Mokrab, and Catherine Venién-Bryan for useful discussions.

SUPPORTING INFORMATION AVAILABLE

Sequence alignment, analysis of side chain torsion angles during MD, and tables of molecular dynamics details. This material is available free of charge via the Internet at http://pubs.acs.org.

REFERENCES

1. Lopatin, A. N., and Nichols, C. G. (2001) Inward rectifiers in the heart: an update on I_{K1}. *J. Mol. Cell. Cardiol. 33*, 625–638.
2. Tamargo, J., Caballero, R., Gómez, R., Valenzuela, C., and Delpón, E. (2004) Pharmacology of cardiac potassium channels. *Cardiovasc. Res. 62*, 9–33.
3. van Wagoner, D. R. (2003) Electrophysiological remodeling in human atrial fibrillation. *Pacing Clin. Electrophysiol. 26* (Part 2), 1572–1575.
4. Stanfield, P. R., and Sutcliffe, M. J. (2003) Spermine is fit to block inward rectifier (Kir) channels. *J. Gen. Physiol. 2003*, 481–484.
5. Stanfield, P. R., Davies, N. W., Shelton, P. A., Sutcliffe, M. J., Khan, I. A., Brammar, W. J., and Conley, E. C. (1994) A single aspartate residue is involved in both intrinsic gating and blockage by Mg2+ of the inward rectified, IRK1. *J. Physiol. 478*, 1–6.
6. Kuo, A. L., Domene, C., Johnson, L. N., Doyle, D. A., and Vénien-Bryan, C. (2005) Two different conformational states of the KirBac3.1 potassium channel revealed by electron crystallography. *Structure 13*, 1463–1472.
7. Pegan, S., Arrabit, C., Slesinger, P. A., and Choe, S. (2006) Andersen's syndrome mutation effects on the structure and sssembly of the cytoplasmic domains of Kir2.1. *Biochemistry 45*, 8599–8606.
8. Pegan, S., Arrabit, C., Zhou, W., Kwiatkowski, W., Collins, A., Slesinger, P. A., and Choe, S. (2005) Cytoplasmic domain structures of Kir2.1 and Kir3.1 show sites for modulating gating and rectification. *Nat. Neurosci. 8*, 279–287.
9. Haider, S., Khalid, S., Tucker, S. J., Ashcroft, F. M., and Sansom, M. S. P. (2007) Molecular dynamics simulations of inwardly rectifying (Kir) potassium channels: a comparative study. *Biochemistry 46*, 3643–3652.
10. Nishida, M., Cadene, M., Chait, B. T., and MacKinnon, R. (2007) Crystal structure of a Kir3.1-prokaryotic Kir channel chimera. *EMBO J. 26*, 4005–4015.
11. Clamp, M., Cuff, J., Searle, S. M., and Barton, G. J. (2004) The Jalview Java alignment editor. *Bioinformatics 20*, 426–427.
12. Edgar, R. C. (2004) MUSCLE: Multiple sequence alignment with high accuracy and high throughput. *Nucleic Acids Res. 32*, 1792–1797.
13. Eswar, N., Webb, B., Marti-Renom, M. A., Madhusudhan, M. S., Eramian, D., Shen, M.-y., Pieper, U., and Šali, A. (2006) Comparative Protein Structure Modeling Using Modeller. In *Current Protocols in Bioinformatics*; John Wiley & Sons: New York.
14. Laskowski, R. A., MacArthur, M. W., Moss, D. S., and Thornton, J. M. (1993) PROCHECK: A program to check the stereochemical quality of protein structures. *J. Appl. Crystallogr. 26*, 283–291.
15. Humphrey, W., Dalke, A., and Schulten, K. (1996) VMD: Visual Molecular Dynamics. *J. Mol. Graphics 14*, 33–38.

16. Kleywegt, G. J., and Jones, T. A. (1994) Detection, delineation, measurement and display of cavities in macromolecular structures. *Acta Crystallogr. D50*, 178–185.
17. Jogini, V., and Roux, B. (2005) Electrostatics of the intracellular vestibule of K^+ channels. *J. Mol. Biol. 354*, 272–288.
18. Baker, N. A., Sept, D., Joseph, S., Holst, M. J., and McCammon, J. A. (2001) Electrostatics of nanosystems: Application to microtubules and the ribosome. *Proc. Natl. Acad. Sci. U.S.A. 98*, 10037–10041.
19. Beckstein, O., Tai, K., and Sansom, M. S. P. (2004) Not ions alone: Barriers to ion permeation in nanopores and channels. *J. Am. Chem. Soc. 126*, 14694–14695.
20. Smart, O. S., Neduvelil, J. G., Wang, X., Wallace, B. A., and Sansom, M. S. P. (1996) HOLE: A program for the analysis of the pore dimensions of ion channel structural models. *J. Mol. Graphics 14*, 354–360.
21. Rashin, A. A., and Honig, B. (1985) Reevaluation of the Born model of ion hydration. *J. Phys. Chem. 89*, 5588–5593.
22. Dolinsky, T. J., Nielsen, J. E., McCammon, J. A., and Baker, N. A. (2004) PDB2PQR: An automated pipeline for the setup of Poisson−Boltzmann electrostatics calculations. *Nucleic Acids Res. 32*, W665–W667.
23. Wang, J., Cieplak, P., and Kollman, P. A. (2000) How well does a restrained electrostatic potential (RESP) model perform in calculating conformational energies of organic and biological molecules? *J. Comput. Chem. 21*, 1049–1074.
24. van der Spoel, D., Lindahl, E., Hess, B., Groenhof, G., Mark, A. E., and Berendsen, H. J. C. (2005) GROMACS: Fast, Flexible and Free. *J. Comput. Chem. 26*, 1701–1718.
25. Bond, P. J., Holyoake, J., Ivetac, A., Khalid, S., and Sansom, M. S. P. (2007) Coarse-grained molecular dynamics simulations of membrane proteins and peptides. *J. Struct. Biol. 157*, 593–605.
26. Berendsen, H. J. C., Postma, J. P. M., van Gunsteren, W. F., DiNola, A., and Haak, J. R. (1984) Molecular-Dynamics with coupling to an external bath. *J. Chem. Phys. 81*, 3684–3690.
27. Darden, T., York, D., and Pedersen, L. (1993) Particle mesh Ewald: An *N* log *N* method for Ewald sums in large systems. *J. Chem. Phys. 98*, 10089–10092.
28. Murdock, S. E., Tai, K., Ng, M. H., Johnston, S., Wu, B., Fangohr, H., Laughton, C. A., Essex, J. W., and Sansom, M. S. P. (2006) Quality assurance for biomolecular simulations. *J. Chem. Theory Comput. 2*, 1477–1481.
29. Fowler, P., Khalid, S., Mokrab, Y., Sansom, M. S. P., Stansfeld, P., and Tai, K. (2008) KDB: A potassium channel model and simulation database. *Biophys. J. 94*, 2038.
30. Tai, K., Murdock, S., Wu, B., Ng, M. H., Johnston, S., Fangohr, H., Cox, S. J., Jeffreys, P., Essex, J. W., and Sansom, M. S. P. (2004) BioSimGrid: Towards a worldwide repository for biomolecular simulations. *Org. Biomol. Chem. 2*, 3219–3221.
31. Schuettelkopf, A. W., and van Aalten, D. M. F. (2004) PRODRG: A tool for high-throughput crystallography of protein-ligand complexes. *Acta Crystallogr. D60*, 1355–1363.
32. Wallace, A. C., Laskowski, R. A., and Thornton, J. M. (1995) LIGPLOT: A program to generate schematic diagrams of protein-ligand interactions. *Protein Eng. 8*, 127–134.
33. Vriend, G. (1990) WHAT IF: A molecular modeling and drug design program. *J. Mol. Graphics 8*, 52–56.
34. Morris, G. M., Goodsell, D. S., Halliday, R. S., Huey, R., Hart, W. E., Belew, R. K., and Olson, A. J. (1998) Automated docking using a Lamarckian genetic algorithm and and empirical binding free energy function. *J. Comput. Chem. 19*, 1639–1662.
35. Robertson, J. L., Palmer, L. G., and Roux, B. (2008) Long-pore electrostatics in inward-rectifier potassium channels. *J. Gen. Physiol. 132*, 613–632.
36. Kurata, H. T., Cheng, W. W., Arrabit, C., Slesinger, P. A., and Nichols, C. G. (2007) The role of the cytoplasmic pore in inward rectification of Kir2.1 channels. *J. Gen. Physiol. 130*, 145–155.
37. Lopatin, A. N., Makhina, E. N., and Nichols, C. G. (1995) The mechanism of inward rectification of potassium channels: "long-pore plugging" by cytoplasmic polyamines. *J. Gen. Physiol. 106*, 923–955.
38. Stansfeld, P. J. (2007) Molecular modelling of potassium channels. Ph.D. Thesis, University of Leicester, Leicester, England.
39. Taglialatela, M., Ficker, E., Wible, B. A., and Brown, A. M. (1995) C-terminus determinants for Mg^{2+} and polyamine block of the inward rectifier K^+ channel IRK1. *EMBO J. 14*, 5532–5541.
40. Yang, J., Jan, Y. N., and Jan, L. Y. (1995) Determination of the subunit stoichiometry of an inwardly rectifying potassium channel. *Neuron 15*, 1441–1447.
41. Xie, L.-H., John, S. A., and Weiss, J. N. (2002) Spermine block of the strong inward rectifier potassium channel Kir2.1: dual roles of surface charge screening and pore block. *J. Gen. Physiol. 120*, 53–66.
42. Kubo, Y., and Murata, Y. (2001) Control of rectification and permeation by two distinct sites after the second transmembrane region in Kir2.1 K^+ channel. *J. Physiol. 531.3*, 645–660.
43. Fujiwara, Y., and Kubo, Y. (2006) Functional roles of charged amino acid residues on the wall of the cytoplasmic pore of Kir2.1. *J. Gen. Physiol. 127*, 401–419.